Multimodal two-phase flow measurement using dual plane ECT and GRT

Stian H. Stavland, Yessica Arellano, Andy Hunt, Rachid Maad, and Bjørn T. Hjertaker

***Abstract*— The present work assesses the accuracy two phase flow measurement, based on cross-correlation and cross-spectrum velocity computation, using dual plane non-intrusive Electrical Capacitance Tomography (ECT), over a broad spectrum of horizontal flow configurations, combined with fraction distribution measurements from Gamma-ray Tomography (GRT). The measurement of two-phase flow encompasses the measurement of both the velocity and the phase concentration of the flow components. The accuracy of the flow velocity is still an open discussion and remains a key challenge in the field of multiphase flow measurement. The velocities of the two-phase components vary, both in between them, and across the pipe cross-section. This study assesses the use of cross- correlation techniques as methods for calculating the cross-sectional velocity distribution by deriving the transit time of the fluid flowing through two parallel ECT sensor arrays mounted on the perimeter of a pipe. The spectral distribution of the velocities is assessed for improved accuracy of individual component velocities. A dual-plane ECT is adopted for the velocity measurements and are combined with state-of-the-art density-based cross-sectional phase fraction distribution from a GRT system to measure the volumetric flow rates of the two phases. The results show that the cross-spectrum method provides enhanced velocity estimation for both flow phases over the conventional cross-correlation technique. Further improvement was reported using a simple predictive correction model resulting in flowrate estimation accuracy of ±10%.The method for two-phase flow measurement suggested in this work leverages the accuracy of the tomography systems on accurate fraction measurement and fast data acquisition to lead to potential enhancement in process control by enabling a more accurate prediction of components velocities.**

***Index Terms*—Multimodal sensors, Electrical capacitance tomography, Gamma-rays, Tomography, Fluid flow measurement**

I. Introduction

MULTIPHASE flow, the combined flow of gas, liquids, and or solids, is inherently complex. Even at a macroscopic level, the properties of the flow vary greatly, both temporally and spatially, depending on the operation parameters and fluid properties. Multiphase flow entails interaction between the different phases, which yields momentum and mass transfer, dynamic phase distributions, and varying interfacial forces. The measurement and analysis of multiphase flow is, hence, complex. Multiphase flow measurement involves the measurement of the individual component velocities and fractions to give an accurate volumetric flow rate. If the mass flow is to be determined, the density of the components must also be known.

Depending on the measurement principle, the accuracy of the flow meters has been found to be strongly affected by the fluid properties and process conditions. Despite this, inline metering of multiphase processes gives valuable information for operators. In the oil and gas industry, the use of multiphase flow meters has had an increased impact in daily operations raging form process optimization to production allocation metering.

There is, however, a drive for better accuracy, which would increase and broaden the potential use of multiphase meters. In this regard, Industrial Process Tomography (IPT) has experienced large interest and development in the past decades due to its non-invasive characteristics, low costs, speed, and size flexibility [1]. IPT technologies have the ability to measure the cross-sectional phase distribution and to identify flow patterns [2] [3], which could potentially be used in conjunction to develop a generalised approach to multiphase metering.

Current IPT research trends show an increasing interest in multi-modal and multi-spectral imaging methods that address various process monitoring and metering problems. Dual-modality tomography leverages the strengths of each measurement method, by complementing each other, hence improving sensitivity to various quantities, and cancelling their stand-alone limitations as, for example, low spatial or temporal resolution [4].

The present work is an extension of the proceedings paper [5], which exploits two-phase flow measurements from Gamma-ray tomography (GRT) and Electrical Capacitance Tomography (ECT). GRT, based on radiation attenuation, is well studied for determination of the gas fraction distribution non-intrusively in two-phase gas-liquid flows, e.g. stratified gas-oil flows, and gas-solid flows [6] [7]. GRT offers advantages over other radiation attenuation methods, as it is less expensive than neutron-densitometry and provides monochromatic radiation without the intensity fluctuations reported in X-ray attenuation techniques [8]. GRT measurements are combined in this work with ECT. ECT is a soft tomography technique that has been largely used for imaging and velocity measurement of non-conducting two-phase flows [9] [10]. The applications of ECT have proved highly accurate in oil-gas metering [11] [12] and mixtures with low water cuts [13]. The dual-modality setup exploits the measurement of different physical quantities of the fluids, i.e. density and electrical permittivity, and leverages on the high-speed acquisition rate of ECT, which enables velocity measurements on flow structures with high frequency variations, and the high spatial accuracy of the GRT.

This work addresses correlation techniques [14] [15], employed for measurement of velocity from a two-plane ECT system. For this, the time delay of fluctuating signals measured at two separate locations are used to obtain a velocity measurement. The cross-correlation technique used has been broadly studied in the literature and proved to be a useful tool for pipeline velocity measurement [16] [17]. The approaches

This is the accepted version of an article published in IEEE Transactions on Instrumentation and Measurement
http://dx.doi.org/10.1109/TIM.2020.3034615

taken by various authors are diverse, ranging from assessment of time series of cross-sectionally averaged void fractions [18] to the study of the motion of interfaces of fluid structures for varying cross-sectional arrangements [2], encompassing either raw data or reconstructed images. Conducted research shows that the cross-correlation velocity is a structural velocity, which departs from the mixture velocity depending on the flow parameters, e.g. flowrate and ratio of inertial to gravity forces. The cross-spectrum technique is related to the cross-correlation, but has not been applied to two-phase flow measurement, to the authors' knowledge. In this application, the phase of the complex cross-spectrum is used to estimate the velocity. This enables the possibility to evaluate whether there is a frequency dependence for the measured velocity. If different types of structures, e.g., slugs, gas bubbles, or liquid droplets, travel at different velocities and have different frequency signatures. This may then affect the velocity spectrum and enable a method to better discern the velocity of the individual flow components.

The main benefit of using tomographic systems is the possibility to combine local measurements and integrate them over the cross-section. In this work, the multimodal measurements are combined through a zonal sectorization procedure of the reconstructed images from both tomography systems. If the zones with more liquid have a lower velocity than those with a high gas content, and this is reflected in the zonal measurements, the technique will improve the accuracy compared to traditional bulk measurements.

The overarching objective of this work is to progress the development of two-phase flow measurement. Specifically it explores the capability of the measurement system to discern the velocity of the individual flow components, aiming to reduce the traditional limitations by drawing on the individual strengths of GRT and ECT, i.e., improved spatial accuracy from GRT and better temporal resolution from ECT.

The capability to measure the velocity of the individual flow are assessed by examining the accuracy of cross-correlation and cross-spectrum velocity computation over a broad spectrum of horizontal gas-oil flow configurations using dual-plane ECT velocity measurements and GRT-derived phase fractions.

The remainder of the manuscript is divided in three main sections. Section II describe the functionality and measurement principle of the flow meters and details the experimental facility and procedures. Following, Section III discusses the cross-correlation and cross-spectrum velocity measurements and outlines the correlation with the dynamic of the flow phenomena. Finally, the conclusions of the work are drawn in Section IV.

II. Methods

A. *Electrical Capacitance Tomography (ECT)*

The principle of operation of ECT is based on the sensitivity of the instrument to changes in the dielectric properties of the fluids in the pipe. The difference between the permittivity of the components causes variations in the inter-electrode capacitance measurement. Each electrode-pair combination will have an associated sensitivity matrix. The elements in the sensitivity matrix for each electrode pair indicate whether a change in the permittivity of a single pixel inside the ECT sensor will affect the capacitance measured between the electrodes of this pair. Hence, the measurements from the sensors are relational to the distribution of the dielectric properties within the pipe. The liquid volumetric fractions from ECT are calculated from the permittivity measurements using the extended Maxwell-Wagner-Sillars model described in [11] as in (1)

$$\varepsilon_m = \varepsilon_c[1 + n\alpha(\varepsilon_i - \varepsilon_c)/(\varepsilon_i + (n-1)\varepsilon_c - \alpha(\varepsilon_i - \varepsilon_c)] \quad (1)$$

where the ε_m is the effective mixture permittivity, ε_c is the permittivity of the continuous material, ε_i is the permittivity of the inclusions, α is the volumetric fraction occupied by the inclusions, and the coefficient n is a function of the eccentricity of the inclusions, taking a value of 3 for spheres [19] and greater than 3 for prolate spheroids [11].

The ECT sensor head used comprised an array of 16 conducting electrodes, arranged in two parallel measurement planes, clamped on the outside of a non-conductive pipe. The sensor array is fully guarded ensuring that the electric field does not fringe out into the flow and improving the quality of the measurements and reconstructed images [20].

Each sensor array operates by multiplexing measurements between all unique capacitance pairs yielding 28 independent measurements for every time frame. The parallel measurement planes are located 68 mm apart. This separation distance is small enough as to ensure coherence of the flow structures between both measurement planes [21]. The measurements from both planes provide information about the permittivity distribution, i.e. phase fraction distribution, and allows cross-correlation of the dynamic structures in different zones of the cross-section of the pipe. The excitation signal was a square wave of 24 $V_{p\text{-}p}$ at 2.5 MHz. The sampling rate of 2.8 ms allows sufficient temporal resolution to capture the physical phenomena. Details of the ECT sensor are provided in Fig. 1, TABLE I illustrates the sensor head setup.

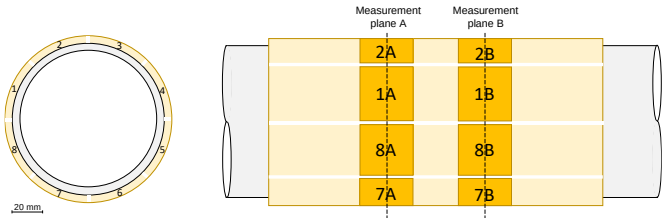

Fig. 1. High-speed Electrical Capacitance Tomography system showing the cross-sectional (left) and longitudinal (right) views. The numeric notation *(1-8)* refers to the ECT sensor index and the notation A and B refers to the measurement plane.

TABLE I. TECHNICAL SUMMARY OF THE ECT

ECT sensor model	APL-S-SL-090
Nominal sensor ID	100 mm
Number of measurement planes	2
Number of electrodes per plane	8
Axial length of measurement electrode	36 mm
Axial separation of measurement planes	68 mm
Capacitance measurement range	6 fF – 400 fF
Measurement resolution	<0.1 fF
Sampling frequency	354 Hz
Excitation frequency (square wave)	2.5 MHz

This is the accepted version of an article published in IEEE Transactions on Instrumentation and Measurement
http://dx.doi.org/10.1109/TIM.2020.3034615

B. Gamma-ray Tomography (GRT)

Gamma-ray tomography is based on gamma densitometry, where a large number of different ray paths are measured through a cross-sectional plane or volume and then reconstructed to an image. In gamma densitometry, the attenuation of gamma radiation through a media is measured to estimate its density. For monochromatic radiation, in the gamma-ray energy range dominated by Compton scattering, the linear attenuation is approximately proportional to the density of the matter. For a narrow beam the measured intensity I in relation to the incident beam intensity I_0, the build-up factor B, the linear attenuation μ and the distance x is given by the Beer-Lambert exponential decay law, as shown in (2) [22].

$$I = BI_0 e^{-\int \mu(x)dx} \tag{2}$$

The average linear attenuation can be found from taking the natural logarithm of the ratio I_0/I and dividing by the length the radiation travel through the medium. For mixtures and compounds, the average linear attenuation is the sum of the products between attenuation and volume fraction of each component assuming a distribution close to homogenous or layered perpendicular to the beam. This assumption generally holds for matter within a narrow beam.

For two component mixtures, it is often more convenient to measure the component fractions. This can be done by normalizing the measured intensity to that of the calibrated measured intensity of the single components, as shown in (3).

$$\alpha_1 = \ln\frac{I_2}{I_m}\Big/\ln\frac{I_2}{I_1} \tag{3}$$

where, I_1 and I_2 are the measured intensities for the single components, α_1 is the volume fraction of the first component and I_m the measured intensity of the mixture.

The high-speed gamma-ray tomography system was designed and prototyped at Department of Physics and Technology, University of Bergen. The design is based on five 500 mCi, 241 Am gamma-ray sources at a principal energy of 59.5 keV, symmetrically mounted around the pipe, as shown in Fig. 2. Corresponding to the five gamma-ray radiation sources, five detector arrays, each consisting of 17 CdZnTe detectors, are mounted on the opposite side of the pipe. CdZnTe semiconductor detectors offer a good signal-to-noise ratio and short response time, in addition to high stopping efficiency at the selected gamma-ray energy. The CdZnTe semiconductor detectors are operated in pulse mode, with a read-out system optimized for high count rates with a peaking time of 200 ns [23].

This yields 85 independent line measurements of the component fractions that is used for the reconstruction of the fraction distribution across the cross-section of the pipe. The tomographic images are reconstructed using an iterative least squares algorithm [27], which gives accurate cross-sectional measurements of the density distribution [24][25][26], and is well suited for fraction measurements in a two-phase gas-liquid flow. Additionally, the bulk component fraction can be measured, without doing any reconstruction [8], leaving out any reconstruction uncertainty.

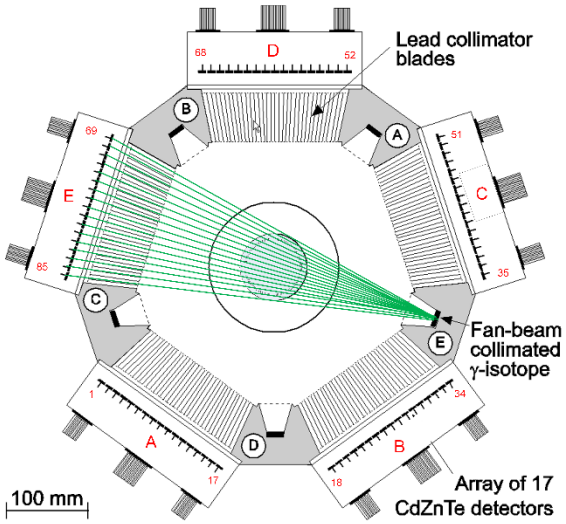

Fig. 2. High-speed gamma-ray tomography system. The notation A, B, C, D and E in the figure refers to gamma radiation source and detector array pairs (views).

C. Velocity measurements

The velocity of a flow can be found through two measurements separated by a known distance along the flow. If the measured signal is fluctuating due to the presence of flow structures, that remain approximately unchanged as flow passes the two measurement points, the flow velocity can be estimated from delay between the two signals. A common method for finding this velocity is to do a cross-correlation of the two signals. In this work cross-correlation along with phase measurement, using the cross-spectrum technique, are explored. Taking advantage of the tomographic method, the cross-section can be divided into zones that are correlated individually resulting in a velocity distribution.

The cross-correlation velocity function (R_{xy}) is defined in (4). Where $x(t)$ and $y(t)$ are the instantaneous measurements and T is the integration time. If two signals are correlated, with a certain delay, the cross-correlation will have a peak at a delay τ_{peak}.

$$R_{xy}(\tau) = \lim_{T\to\infty}\frac{1}{T}\int_0^T x(t)y(t+\tau)dt \tag{4}$$

For flow measurement application of the cross-correlation will be applied to a finite number of samples. Either the time series will be divided into sections or a moving window is applied. The discrete form of the cross-correlation is given in (5)

$$R_{xy}(n) = \frac{1}{N}\sum_{i}^{N} x(i)y(i+n) \tag{5}$$

where n is the number of samples delayed and N is the correlation sample length. Additionally, the cross-correlation mean of the signals are subtracted and the results normalized.

This is the accepted version of an article published in IEEE Transactions on Instrumentation and Measurement
http://dx.doi.org/10.1109/TIM.2020.3034615

A fit is used on the peak to improve the accuracy of the peak location.

The phase of the cross-spectrum of two correlated signals is dependent on the delay between them. Subsequently, the frequency dependence of the delay can also be resolved. The cross-spectrum can be calculated from the complex frequency spectrum of two signals taking the dot product of the conjugated of the first signal with the other [14] as shown in (6).

$$S_{AB}(f) = A^*(f) \cdot B(f) \tag{6}$$

where f is the frequency, S_{AB} is the cross-spectrum, and A and B are the measured spectra of the two measuring points. The frequency-dependent delay between the signals is found by dividing the phase of the spectrum on the frequency. Dividing the distance between measuring points on the delay yields the velocities as shown in (7).

$$v_{AB}(f) = \frac{l_{AB}}{\Delta t_{AB}(f)} = \frac{2\pi f l_{AB}}{\angle S_{AB}(f)} \tag{7}$$

where v is the velocity, l is the length, and Δt is the delay. By estimating the auto spectra, S_{AA} and S_{BB}, of the two signals and averaging multiple spectra, the coherence spectrum γ_{AB} can also be found, as shown in (8). By setting an appropriate threshold for the coherence this can be used to filter the delay estimates from the cross-spectrum.

$$\gamma_{AB}^2 = \frac{|S_{AB}(f)|^2}{S_{AA}(f) \cdot S_{BB}(f)} \tag{8}$$

For a flow measurement application, the delay estimate must be discretized in time. In this regard, the so-called 'Welch method' [15] has been employed, where the measured signals are divided into partially overlapping segments before the cross-spectrum is calculated. Additionally, before calculating the spectra, the average DC components of the signals are removed, and the edges of the segments are tapered with a Hann window. The Hann window is a so-called raised cosine window, which with a 50 % overlap, results in equal weight to all samples. The computation of the cross-spectrum is then shown in (9).

$$\begin{aligned} \bar{S}_{AB_K}(n) &= \sum_j^N S_{AB_j}(n) = \sum_j^N A_j^*(n) \cdot B_j(n) \\ &= \sum_j^N \mathcal{F}^*\{w(i)(a(i)_j - \bar{a}_j)\} \cdot \mathcal{F}\{w(i)(b(i)_j - \bar{b}_j)\} \end{aligned} \tag{9}$$

where a_j and b_j are the signal the j[th] signal segment, and w is the Hann window.

Different type of structures, e.g. slugs, gas bubbles, or liquid droplets, may travel at different velocities, and have different frequency signatures. The different velocity rates could potentially be detected and measured using the cross-spectrum methods. Without knowing the frequency signatures of the various structures, nor which structures are coherent, or not, from one measurement plane to the next, a high-level approach is chosen in this study.

Fig. 3 illustrates the frequency spectrum divided in two, i.e. a high-frequency range and a low-frequency range. The high-frequency range is limited by a maximum frequency to avoid high-frequency noise interfering. The maximum frequency is chosen based on the typical high coherence range. The split frequency is selected based on observation of the velocity spectra, where there seems to be more variation in the low-frequency end and a less varying trend as the frequency increases. Since the frequency of the signals is expected to scale by the velocity, the frequency split and the maximum frequency are scaled accordingly. This scaling is readily apparent for the frequency range of the randomly chosen spectra (in grey) shown in Fig. 3. From the two sections statistical data as maximum, minimum, mean, median, etc., can be extracted and correlated to actual flow velocities.

D. Combining GRT and ECT

Before combining the different modalities, both GRT and ECT measurements are reconstructed on a 32 by 32-pixel matrix. In this study, two separate correlation configurations have been used, i.e., a full cross-section conventional setup and a zonal discretization. The second approach comprises the division of the pipe cross-section into zones. The zonal division enables the cross-correlation of individual zones and, thereby, the cross-sectional velocity distribution. Zonal discretization simplifies the velocity distribution calculation by reducing the number of areas needed to be correlated. By averaging over the pixels included in the zone, the noise level is also reduced, giving improved robustness of the velocity estimation.

When selecting a zonal configuration, the size of the zones needed to improve signal strength must be weighed against the spatial resolution ensuring that necessary information is not lost [3]. Different zonal configurations have been assessed in the past, where particular configurations allow obtaining velocity profiles along certain symmetrical axis depending on the flow structure [2]. Given the broad range of flow conditions under

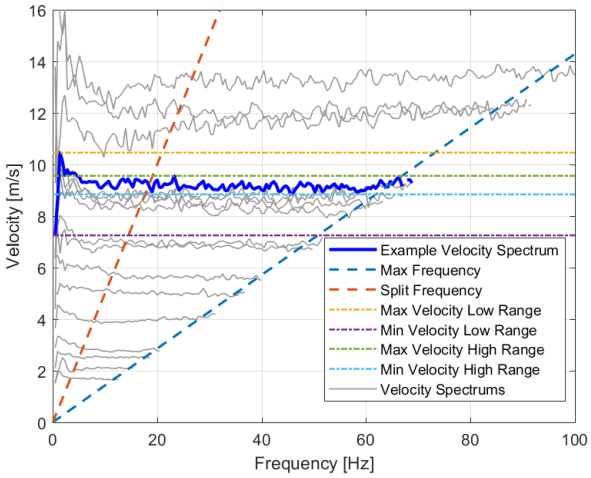

Fig. 3. Example velocity spectrum with added lines indicating high and low-frequency range and the corresponding min and maximum values. Also included randomly chosen velocity spectra at different flow rates to illustrate the variance. The spectra are filter by coherence threshold.

This is the accepted version of an article published in IEEE Transactions on Instrumentation and Measurement
http://dx.doi.org/10.1109/TIM.2020.3034615

assessment in this work, yielding various flow configurations, a 13-zone configuration was used, illustrated in Fig. 4.

The ECT and GRT measurements are combined, as in (10), to estimate the gas and liquid flow rates and the zonal distribution of these over the pipe cross-section.

$$Q_i = \sum_{k=1}^{K} Q_{ik} = \sum_{k=1}^{K} \alpha_{ik} v_{ik} A_k \tag{10}$$

where Q_i is ith component volume flow rate, α_{ik} and v_{ik} are the ith component fraction and velocity in the kth zone and A_k is the area of the kth zone. The component fractions are estimated from the GRT measurements and the velocities from ECT measurements.

Since the flow rate of the ith component within each zone is a linear combination of the zonal velocity, component fraction, and area, the relative uncertainty contribution to the zonal flow rate from each variable is the same as the relative uncertainty of the variable. When combining the uncertainties from individual zones it is probable that some of these are correlated. Assuming the area uncertainties are negligible, the combined uncertainties can be expressed as in (11) [28], where the uncertainties are marked u, the correlation factors r and the number of zones N.

$$u_{Q_i}{}^2 = \sum_{k=1}^{N}\sum_{m=1}^{N} A_k A_m \Big(\alpha_{ik}\alpha_{im} u_{v_{ik}} u_{v_{im}} r(v_{ik}, v_{im}) + v_{ik} v_{im} u_{\alpha_{ik}} u_{\alpha_{im}} r(\alpha_{ik}, \alpha_{im}) + 2\alpha_{ik} v_{im} u_{v_{ik}} u_{\alpha_{im}} r(v_{ik}, \alpha_{im})\Big) \tag{11}$$

The zonal uncertainty of the fraction measurements is expected to be in the order of a few present, at least when averaged, and smaller than that of the velocity. The velocity of the correlated flow structures is not necessarily the velocity of either flow component e.g. a wave on a gas liquid interface, powered by the gas, having a higher velocity than the liquid, travels faster than the liquid but slower than the gas.
The zonal fraction measurements are expected to be weakly correlated, both among themselves and with the velocity measurements. The zonal velocity measurements on the other hand are likely more correlated, being largely influenced by changes in flow patterns. That is, large flow structures cover multiple zones and smaller ones have similar attributes in different zones. Still, the averaging effect of using a zonal discretization is expected to improve the overall uncertainty compared to bulk measurements.

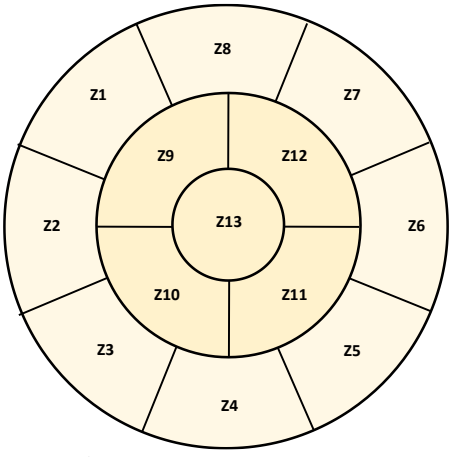

Fig. 4. Configuration of *the* zonal cross-section discretisation.

The more comprehensive analysis of the multimodal setup also requires the assessment of the temporal resolution of the measurements. The permittivity spatial distributions reconstructed from the ECT measurements were taken at a rate of 354 frames per second. Conversely, the sampling rate of the GRT is restricted to 50Hz. The permittivity and velocity measurements then had to be downsampled to match the fraction measurements from the GRT. However, the results in this study are averaged over a significantly longer period, and any temporal effects are not studied in detail.

E. Multiphase flow rig

The experiments were conducted at NORCE Technology in Bergen, Norway. The test facility comprises a recirculating three-phase pressurized flow loop with a gravimetric separator for separation of fluids in continuous operation. The phase separator has a 32 m^3 capacity, and typically contains around 10 m^3 of diesel.

In the tests, diesel and nitrogen gas were used as test fluids. The liquid flow was recirculated around the test facility using centrifugal pumps. The reference liquid flow rate was measured downstream the pump using a designated Coriolis meter for liquid flow. The gas, supplied from a compressor facility, was added further downstream through a standard tee connection. The gas flow rate was also measured using a designated

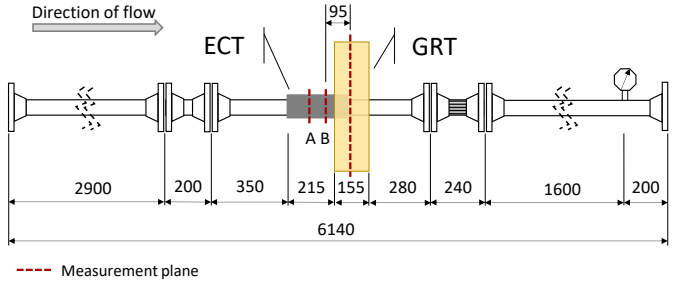

Fig. 5. Schematic of the multiphase test section at NORCE showing the location of tomography systems and pressure measurement point downstream the meters (all dimensions in mm).

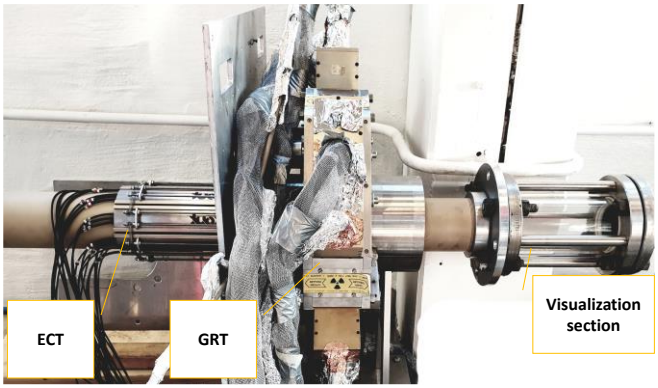

Fig. 6. Gamma-ray tomography (GRT) and electrical capacitance tomography (ECT) systems installed on the experimental test section.

This is the accepted version of an article published in IEEE Transactions on Instrumentation and Measurement
http://dx.doi.org/10.1109/TIM.2020.3034615

Coriolis flowmeter before being mixed with the liquid. The uncertainty of the Coriolis flow meter is 1 % relative within the measurement range.

The rig is instrumented to provide reference measurements of phase fractions, flow rates, pressure, and temperature of all fluids. The experiments were conducted at room temperature with fluid temperatures around 20 °C.

The diagram of the test section in Fig. 5 illustrates the relative positions of the GRT unit and the ECT sensors. The metering devices were co-located in the same horizontal section, with the second ECT measurement plane placed 95 mm upstream the GRT measuring plane. A picture of the installation is shown in Fig. 6.

F. *Experimental procedure*

During the experiment 97 test points were measured, the experimental matrix and flow conditions are summarised in TABLE II. The experimental campaign covered a broad set of Gas-Liquid flow rates, ranging from of 2 to 200 m^3/h for gas and oil, with superficial velocities of 0.1-9.8 and 0.1-4.2 m/s, respectively.

Prior to the flow tests, the ECT and GRT systems were calibrated using the test fluids in single phase as reference for high and low measurement values. The calibration procedure allows the systems to adjust to the specific electrical permittivity and density encountered for the liquid and gas used during the tests. The calibrations were undertaken by alternatively filling the test section with diesel only, and subsequently with nitrogen gas only. For reference, calibration measurements were also conducted after the experiments were concluded.

For each test point the designated flowrates were set and allowed to settle. Next, through the ECT and GRT systems, capacitance and linear attenuation measurements were respectively acquired for around 180 s for each test point. Following completion of the data acquisition the raw data measurements were checked to validate the quality of the measurements. The analysis of the data was completed *a posteriori*.

III. RESULTS AND DISCUSSION

To assess the component velocity measurements, the actual, or "reference" component velocity ($v_{i_{ref^*}}$) is needed. This is not measured directly by the reference metering, but can be estimated by dividing the reference component flow rate ($Q_{i_{ref}}$) by the cross-sectional area (A) and component fraction (α_i), from the GRT, as in (12).

TABLE II. SUMMARY OF EXPERIMENTAL CAMPAIGN

Oil Flow rate (m^3/h)	5-85
Gas Flow rate (m^3/h)	2-200
Gas-Liquid Ratio	30-85
Pressure (bar)	5-8
Temperature (°C)	20
Oil superficial velocity (m/s)	0.1 – 4.2
Gas superficial velocity (m/s)	0.1 – 9.8
Oil density (kg/m^3)	813
Oil relative permittivity	2.2

$$v_{i_{ref^*}} = \frac{Q_{i_{ref}}}{\alpha_i A} \tag{12}$$

When estimating the reference component velocity from the flow rate as described in (12), care must be taken regarding the uncertainty. By assuming negligible contribution from the cross-sectional area, the relative uncertainty of the component velocities can be expressed as in (13).

$$\frac{u_{v_{i_{ref^*}}}}{v_i} = \sqrt{\left(\frac{u_{Q_{i_{ref}}}}{Q_i}\right)^2 + \left(\frac{u_{\alpha_i}}{\alpha_i}\right)^2} \tag{13}$$

where $u_{v_{i_{ref^*}}}$, $u_{Q_{i_{ref}}}$ and u_{α_i} is the uncertainty of the i[th] velocity component, i[th] component flow rate and i[th] component fraction respectively.

Using the relative uncertainty of ($Q_{i_{ref}}$) from the flow rig of 1 %, and the absolute uncertainty of the two-phase fraction measurements (u_{α_i}) from the GRT, estimated to be around 1 % [11], we get the relative uncertainty for $v_{i_{ref^*}}$ as a function of α_i as shown in Fig. 7. When α_i approaches zero the relative uncertainty grows rapidly. For the liquid velocities, it rises from below 2 % around at a liquid fraction of 50 %, to close to 5 % at a 20 % liquid fraction. The gas follows, the same trend, but since there are lower gas fractions in the experimental measurements, it ends up at around 9 %, at a gas fraction of around 10 %.

In the same way as for the reference component velocity($v_{i_{ref^*}}$) above, the component velocity (v_i) from the zonal measurements can be found by dividing the component flow rate (Q_i) by the cross-sectional component fraction (α_i) and area (A). The estimated component flow rate (Q_i) from zonal measurements is calculated as in (10). Combined, the component velocity can be expressed as in (14).

$$v_i = \frac{Q_i}{\alpha_i A} = \frac{1}{\alpha_i}\sum_{k=1}^{K} v_{ik}\alpha_{ik}\frac{A_k}{A} \tag{14}$$

A. *Cross-correlation velocity measurement*

The bulk (average cross-sectional value) measurements and tomographic measurements divided into zones as described in Fig. 4 are compared. The results from the dual-plane ECT system are contrasted to the reference component velocity following as estimated following (12). The results are plotted in

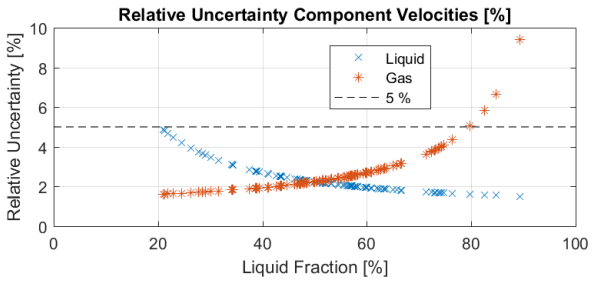

Fig. 7. Relative uncertainty of reference measurement for gas and liquid velocities. Gas shown in red and liquid in blue.

This is the accepted version of an article published in IEEE Transactions on Instrumentation and Measurement
http://dx.doi.org/10.1109/TIM.2020.3034615

Fig. 8, showing the relative errors of the estimated cross-correlation velocities (XC) for the gas and the liquid phases.

The overall trend of the liquid cross-correlation velocities has an inflexion point at a reference liquid velocity of 1.2 m/s. The cross-correlation velocity is approaching the reference value as the liquid velocity increases, while the trend drastically inverses for liquid velocity below 1 m/s. The cross-correlation velocities computed using the zonal discretisation showed enhanced performance over conventional bulk cross-correlation. The gas cross-correlation velocity varies from close to the reference velocity to an underestimation of more than 50 %. There are, however, no clear correlation between the gas velocity and the error.

The association between the superficial phase velocities and the cross-correlation velocities of liquid and gas is further investigated in Fig. 9 and Fig. 10, respectively. The superficial velocities are found by dividing the gas and liquid reference flow rates by the cross-sectional area as shown for superficial gas velocity in (15).

$$v_{Si} = \frac{Q_i}{A} \tag{15}$$

Where v_{Si} is the superficial velocity of the component i, i.e. gas or liquid.

The colour maps for the images are chosen to provide information on the relative deviation between the cross-correlation velocities and the reference velocities. As seen in Fig. 8, there is a clear trend for the cross-correlation liquid velocity to approach the reference liquid velocity (v_L) at higher gas superficial velocities, v_{SG}. Conversely, both superficial velocities of gas and liquid, v_{SG} and v_{SL}, influence the precision of the cross-correlation gas velocity. This is readily evident in the large deviations seen at high v_{SG} and low-to-medium v_{SL}.

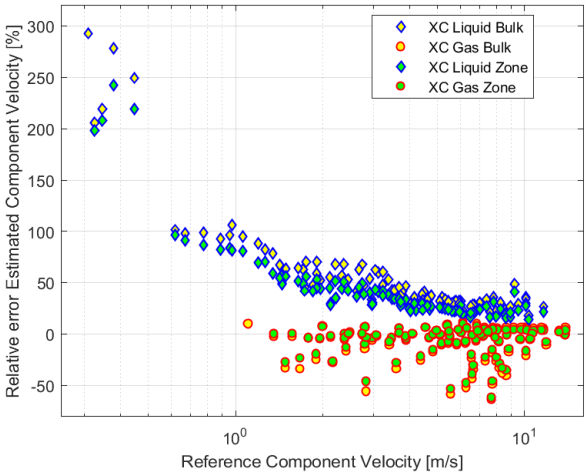

Fig. 8. Relative error of gas and liquid velocities estimated from cross-correlation of the entire cross-section (bulk) and zonal ECT measurements. Data from liquid is shown in diamonds and from gas in circles. Reference component velocity on x-axis.

B. *Cross-spectrum velocity measurement*

From the results above, the cross-correlation method is more effective in predicting the gas phase velocity than that of the liquid phase. The liquid velocity (v_L) tends to be overestimated. This could be caused by the treatment of the method to the flow as a structural velocity propagated along with the gas-liquid mixture. This approach overlooks the flow structures that are propelled by the gas phase through the measurement planes at a greater velocity than the liquid.

The aim, then, is to find a method that enables the correlation, if any, of flow structures moving with the same velocity as the liquid. The cross-spectrum velocity is a candidate in this regard. Considering that the liquid is most likely flowing at a lower or equal velocity to the gas, and as indicated by the cross-correlation velocity measurements, the flow structures travel at speeds somewhere in-between the gas and the liquid velocity, we are most likely looking for correlations of the flow structures traveling at the lowest speed range. Hence, a method where the minimums in the velocity spectrum are identified and used was undertaken. At each test point, and for each zone, the minimum liquid velocity rates are computed, considering three different frequency ranges, i.e., high-frequency, low-frequency, and the entire frequency spectrum. Additionally, the mean of the high-frequency range of the velocity spectra are also found in order to estimate the gas velocity and for comparison of the liquid velocities.

The results plotted in Fig. 11 show the relative error of the liquid velocities estimated from the cross-spectrum (CS). The same inflection point seen for liquid cross-correlation velocity (XC) in Fig. 8 is present for all CS velocities, regardless of the method used. The similarities between the minimum-high frequency CS velocities and the XC velocities are evident, with the cross-spectrum showing a slightly enhanced precision. The cross-spectrum velocities computed using the minimum velocity values of both the low-frequency range and the overall spectrum show an overall lower relative error for reference liquid velocities above 2 m/s. The results, however, are more largely scattered.

Fig. 12 and Fig. 13 show the deviation in the cross-spectrum velocities of liquid and gas, respectively. The colour maps reflect the range of the percentage deviation between the cross-spectrum velocities. As also evident in the cross-correlation velocity data, the higher the liquid superficial velocity the lower the cross-spectrum velocity deviation, as per Fig. 12. A larger deviation in the computed gas velocity is also evident at high gas superficial velocities, marked in blue in Fig. 13.

This is the accepted version of an article published in IEEE Transactions on Instrumentation and Measurement
http://dx.doi.org/10.1109/TIM.2020.3034615

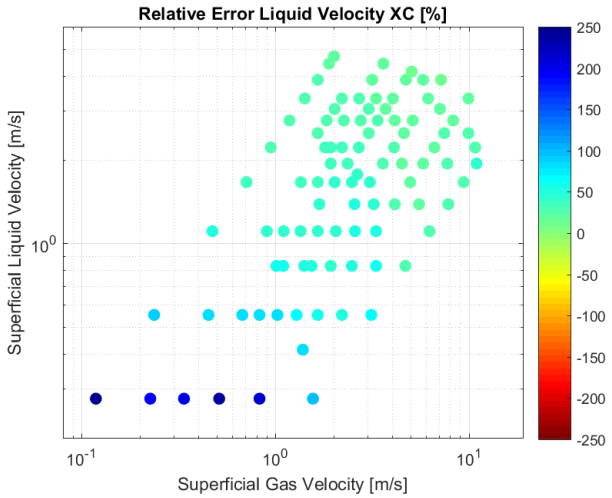

Fig. 9. Relative error of liquid velocities estimated from cross-correlation of zonal ECT measurements. The error is plotted as intensity (colour) and as function of superficial liquid (y-axis) and gas velocities (x-axis).

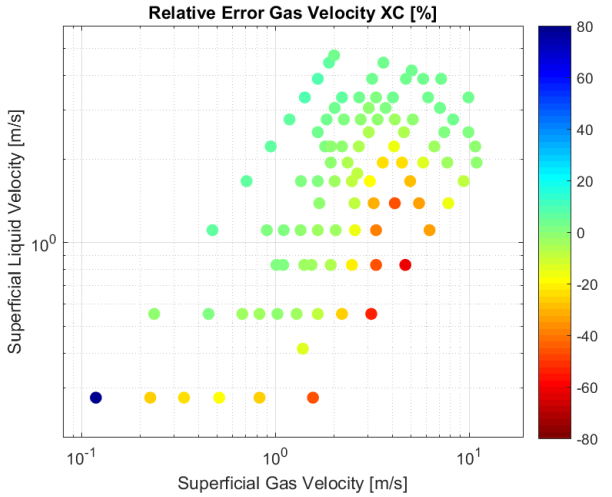

Fig. 10. Relative error of gas velocities estimated from cross-correlation of zonal ECT measurements. The error is plotted as intensity (colour) and as function of superficial liquid (y-axis) and gas velocities (x-axis).

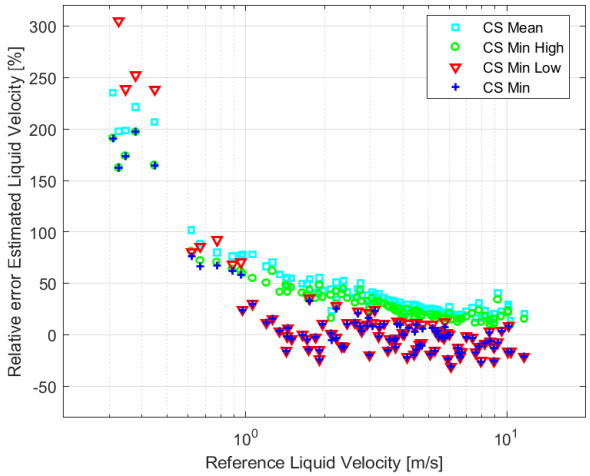

Fig. 11. Relative error of the liquid velocities estimated from cross-spectrum (CS) velocities considering the mean of the high-frequency range (Mean), minimum rate within the high-frequency range (Min-High), low-frequency range (Min-Low) and the entire frequency spectrum (Min) identified with green circles, red triangles, and blue stars, respectively. Reference component velocity on x-axis.

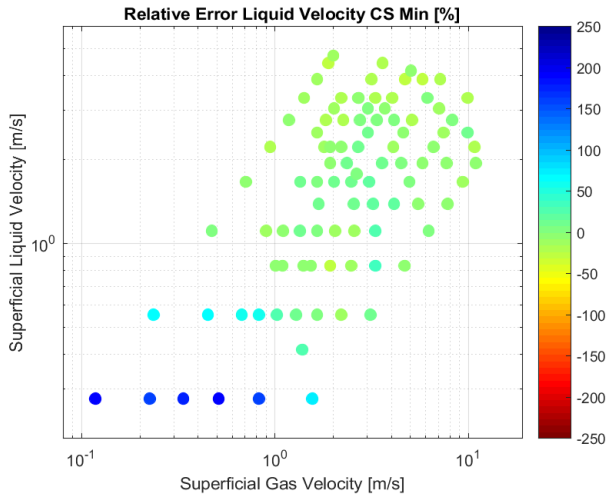

Fig. 12. Relative error of liquid velocities estimated from minimum of entire velocity spectrum and zonal ECT measurements. The error is plotted as intensity (colour) and as function of superficial liquid (y-axis) and gas velocities (x-axis).

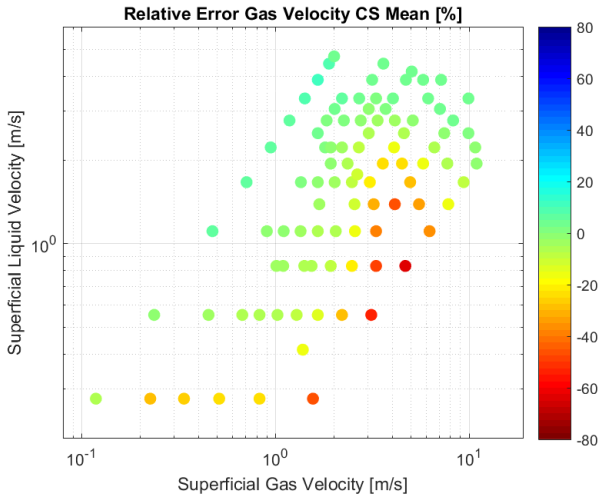

Fig. 13. Relative error of gas velocities estimated from mean of high-frequency range of the velocity spectrum and zonal ECT measurements. The error is plotted as intensity (colour) and as function of superficial liquid (y-axis) and gas velocities (x-axis).

C. Fluid dynamics correlations

The cross-correlation velocity is not the in-situ flow velocity but rather a structural velocity of two-phase flow. The scientific challenge at the moment is to understand that relationship. In order to understand the effects of the flow dynamics on the overall measurement, it is necessary to analyse the slip velocity of the different phases and compare the prediction accuracy of the estimated velocities to the flow patterns developed at relevant operational conditions.

The influence of the slip ratio velocity and slip velocity between the gas and liquid phases for given superficial velocities is investigated in Fig. 14 and Fig. 15, respectively. The slip velocity is larger in the same region where the cross-correlation and cross-spectrum velocity of gas was seen to have the most significant deviations. Similarly, the slip ratio is larger in the same low-velocity regions as the relative deviations in estimated liquid cross-correlation velocity.

A further way of analysing flow structural effects, on the computed structural velocities at gas rates where errors are greater, is through identification of the predominant flow

This is the accepted version of an article published in IEEE Transactions on Instrumentation and Measurement
http://dx.doi.org/10.1109/TIM.2020.3034615

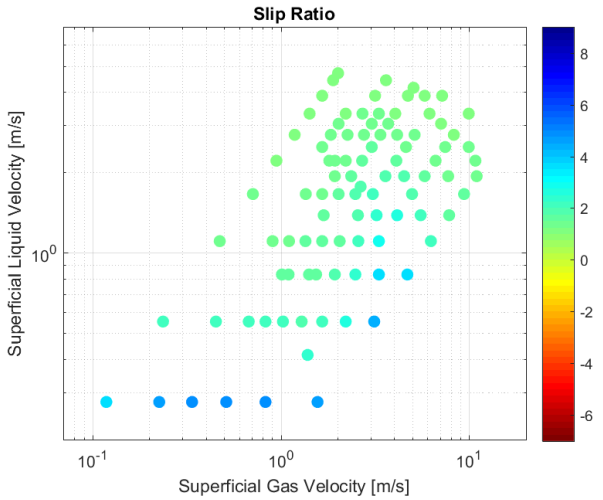

Fig. 14. Slip ratio from the reference liquid and gas velocities. The ratio of gas to liquid velocities is plotted as intensity (colour) and as function of superficial liquid (y-axis) and gas velocities (x-axis).

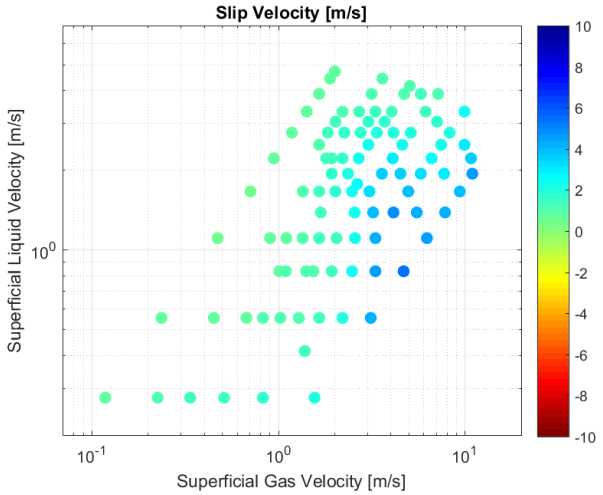

Fig. 15. Slip velocity from the reference liquid and gas velocities. The difference between the gas and liquid velocities is plotted as intensity (colour) and as function of superficial liquid (y-axis) and gas velocities (x-axis).

structures in the vicinity of the region of interest. This was done by identifying the flow regimes from the temporal changes in the cross-section phases based on the density distribution from GRT and the permittivity distribution of ECT, combined with a flow characterisation of the dominant structures from the ECT transient measurements according to the classification parameters listed in [3]. The flow pattern characterisation of test points of interest overlaps the gas cross-spectrum velocity relative error in Fig. 16.

The largest errors in the estimation of the gas velocity take place under stratified flow conditions, where the slip velocity is above 4 m/s. The results show that the presence of periodic structures, i.e. slugs, do significantly enhances the velocity estimation. Also, annular flow was tracked through the measurement planes with the relative same ease as slug flow.

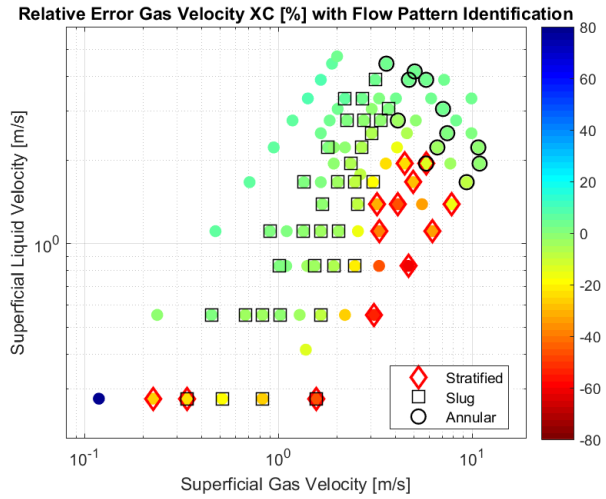

Fig. 16. Flow pattern dominant structures overlapping the relative error of cross-correlation gas velocities plotted as function of superficial liquid (y-axis) and gas velocities (x-axis). The error is plotted as intensity (colour). The flow pattern structures are identified a diamond for slug flow, squares for stratified flow, and dark circles for annular flow.

The deviation of the measurement of liquid velocity using cross-correlation and the minimum of the high-frequency section of the cross-spectrum phase method both falls along a line. This indicates that a predictive model can be used to correct the deviation. To investigate this, a simple linear fit of the form of (16) has been fitted to the results shown in Fig. 17.

$$v_{corr} = k_1 v_{meas} + k_2 \tag{16}$$

where v_{corr} is the corrected velocity, v_{meas} is the measured velocity, and k_1 and k_2 are the correlation coefficients.

Most corrected velocities fall within a ±10% error band even for reference velocities well below the inflection point of 1,2 m/s seen in Fig. 8 and Fig. 11.

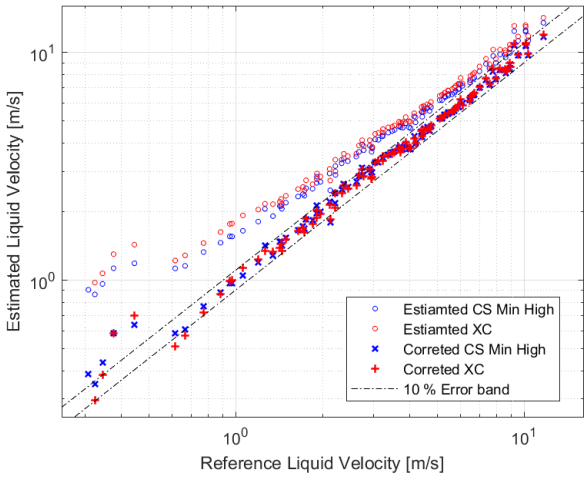

Fig. 17. Liquid velocities estimated using cross-correlation (XC) and cross-spectrum (CS) techniques on zonal ECT measurements and corrected results using predictive model. Initial estimated data shown in circles, and corrected velocities in crosses. Reference component velocity on x-axis.

This is the accepted version of an article published in IEEE Transactions on Instrumentation and Measurement
http://dx.doi.org/10.1109/TIM.2020.3034615

D. *Flow rates*

Building on the analysis above, the liquid and gas flowrates are computed from (10) considering velocities from the cross-correlation (XC) and the cross-spectrum (CS) methods. The estimations using bulk and zonal cross-correlation and cross-spectrum techniques for the liquid flow measurement are presented in Fig. 18 along with flowrate corrections as per (16). The liquid flowrates derived from the cross-spectrum velocity agree with the reference flowrate, particularly for values over 1 m^3/h. The cross-correlation velocity, on the other hand, yields an overestimation of the liquid flowrate, increasing at lower flow rates. The zonal method preforms better than the bulk method but shows the same overall trend. Using the velocity correction model on the estimates form CS minimum from the high-frequency range, the liquid flowrate estimation is improved, matching the reference flowrate within a ±10% margin. These results constitute a significant improvement over the figures previously reported in [5].

The estimations using bulk and zonal cross-correlation and cross-spectrum techniques for gas flow measurement are presented in Fig. 19. As expected from the velocity measurements most of the measurements are aligning up well, but with some measurements underestimating the flow rate. The cross-correlation and the cross-spectrum techniques using zonal measurements performs almost equal, while the bulk cross-correlation technique performs slightly worse, but follows the same trend as the other two.

Since the superficial velocity reported earlier is proportional to the flowrate, the deviation pattern can be observed in Fig. 10 and Fig. 13. Contrasting these with the slip velocity pattern in Fig. 15 and the flow regimes reported in Fig. 16, it is evident that the correlation methods are less accurate when the slip velocity between the gas and the liquid increases. The slip velocity is most significant under stratified flow where the gas flows more unhindered and does not have to move full bore slugs. However, it may be less predictable, from this, that there are not similar deviations in the measurements performed under annular flow regimes, where the slip velocity is also high. Nevertheless, observing the slip ratio in Fig. 14, we see that even though the slip velocity is high in the annular area, the ratio is less. Since the deviation reported is relative to the actual velocity, this might explain why it is less under annular flow condition, which exists at higher flow rates than the stratified.

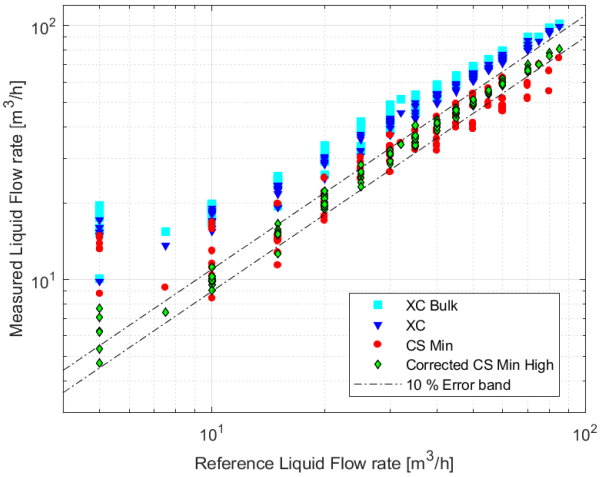

Fig. 18. Liquid flowrates using measured bulk and zonal GRT component fractions combined with corresponding bulk (XC Bulk) and zonal cross-correlation (XC) and zonal cross-spectrum (CS Min) velocity measurements, and the corrected cross-spectrum-velocity (Corrected CS Min High). Reference flowrates on x-axis.

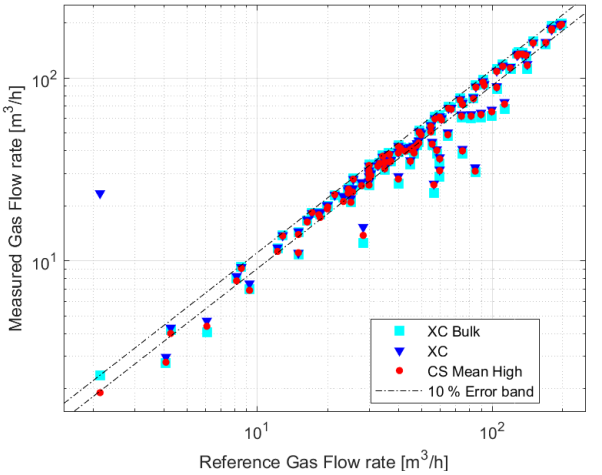

Fig. 19. Gas flowrates using measured bulk and zonal GRT component fractions combined with corresponding bulk and zonal cross-correlation (XC) and zonal cross-spectrum (CS) velocity measurements. Reference flowrates on x-axis.

IV. Conclusion

A series of experiments were conducted on horizontal gas-oil two-phase flow, combining Gamma-ray Tomography (GRT) and Electrical Capacitance Tomography (ECT). The transit time and velocity of the flow structures was obtained by a dual-plane ECT. The estimated velocities were combined with the spatial density-based phase distribution from GRT measurements via a conventional full cross-section correlation and through zonal discretization method. The zonal discretisation of the cross-section resulted in slightly better gas and liquid velocity estimations, when contrasted with bulk cross-correlation measurements.

The study mapped the conditions were velocity estimations were less accurate and targeted the mechanisms behind them. Results indicate that gas cross-correlation velocities show a smaller deviation than liquid cross-correlation velocities over the range of flowrates studied. The largest deviations were seen in stratified flows where the slip velocities surpass 4 m/s.

In search for more accurate velocity measurements of the individual components, cross-spectrum velocities were computed. In doing so, the liquid velocities were calculated for the high and low-frequency range, as well as for the overall frequency spectrum. The cross-spectrum velocity of the liquid phase was significantly improved by using the minimum of the latter two frequency spectra, though at the cost of more scattered results.

A simple predictive model was tested to further improve the liquid velocity prediction and hence the flowrate estimation. Results of this showed accuracy in liquid flowrate measurement within 10% of the reference measurements.

The measurements performed do not cover all possible flow regimes. Notably, bubbly and misty flow was beyond the operational window of the test setup. Wavy stratified flow was

This is the accepted version of an article published in IEEE Transactions on Instrumentation and Measurement
http://dx.doi.org/10.1109/TIM.2020.3034615

covered, with limitations of the setup in the lower end of the flowrate range. However, the experimental campaign still covered a relatively large flow rate envelope, with not insignificant application in relevant processes. There is no indication that the methods discussed should not work beyond the envelope in the high flow rate direction, but there do seem to be larger deviations moving into the stratified flow domain. This responds to the intrinsic less dynamism in the flow as it is dominated by the viscous forces, and hence fewer flow structures to correlate on.

There is potential for the methods discussed to be applied to other processes. However, this would be dependent on some key variables. The first and most important is that the used tomographic method is sensitive to the fluids used, e.g., using Electrical Impedance Tomography (EIT) instead of ECT for conductive fluids. Second, the accuracy-dependence on flow regime structures implies that different flow regimes yielding from variation in the fluid properties, i.e., viscosity and density, and piping setup may limit the system operational envelope. Furthermore, although the results presented are based on horizontal flow configurations, different pipe inclinations would also affect the flow regimes, the method should still be applicable.

REFERENCES

[1] Y. Arellano, O. Haas, H. Ahmed, A. Hunt, and L. Ma, "If cheap and easy oil is over, what now?," in *International Conference on energy and sustainable futures*, 2019, no. 1, pp. 1–7.

[2] R. Drury, A. Hunt, and J. Brusey, "Identification of horizontal slug flow structures for application in selective cross-correlation metering," *Flow Meas. Instrum.*, vol. 66, no. December 2018, pp. 141–149, 2019.

[3] Y. Arellano, A. Hunt, O. Haas, and L. Ma, "On the life and habits of gas-core slugs: characterisation of an intermittent horizontal two-phase flow," *J. Nat. Gas Sci. Eng.*, 2020.

[4] G. Liang, S. Ren, and F. Dong, "An Inclusion Boundary Reconstruction Method Using Electrical Impedance and Ultrasound Reflection Dual-Modality Tomography," in *9th World Congress on Industrial Process Tomography*, 2018, pp. 11–19.

[5] S. H. Stavland, Y. Arellano, A. Hunt, R. Maad, and B. T. Hjertaker, "Multimodal analysis of gas-oil intermittent structures in co-current horizontal flow," in *2020 IEEE International Instrumentation and Measurement Technology Conference (I2MTC)*, 2020, pp. 1–6.

[6] T. Dyakowski, G. A. Johansen, B. T. Hjertaker, D. Sankowski, V. Mosorov, and J. Wlodarczyk, "A Dual Modality Tomography System for Imaging Gas/Solids Flows," *Part. Part. Syst. Charact*, vol. 23, pp. 260–265, 2006.

[7] A. Hunt, J. Pendleton, and Y. Ladam, "Visualisation of two-phase gas-liquid pipe flows using electrical capacitance tomography," in *ESDA2004*, 2004, no. January 2004.

[8] S. H. Stavland, C. Sætre, B. T. Hjertaker, S.-A. Tjugum, A. Hallanger, and R. Maad, "Gas Fraction Measurements using Single and Dual Beam Gamma-Densitometry for Two Phase Gas- Liquid Pipe Flow," in *2019 IEEE International Instrumentation and Measurement Technology Conference (I2MTC)*, 2019, pp. 1–6.

[9] M. Zhang, Y. Li, and M. Soleimani, "Experimental Study of Complex-valued ECT," in *9th World Congress on Industrial Process Tomography*, 2018, pp. 19–24.

[10] X. Zhu, P. Dong, and Z. Zhu, "Gas-solids Flow Measurement in Cyclone Dipleg by Dual-plane Electrical Capacitance Tomography Sensor," in *9th World Congress on Industrial Process Tomography*, 2018, pp. 203–209.

[11] A. Hunt, L. A. Abdulkareem, and B. J. Azzopardi, "Measurement of Dynamic Properties of Vertical Gas-Liquid Flow," *7th Int. Conf. Multiph. Flow*, pp. 1–10, 2010.

[12] R. Yan and S. Mylvaganma, "Flow Regime Identification with Single Plane ECT Using Deep Learning," in *9th World Congress on Industrial Process Tomography*, 2018, pp. 289–297.

[13] A. Hunt, "Industrial Applications of High-speed Electrical Capacitance Tomography," in *9th World Congress on Industrial Process Tomography*, 2018, pp. 857–864.

[14] R. B. Randall, *Frequency Analysis*, 3rd ed. K. Larsen & Son A/S, 1987.

[15] P. D. Welch, "The use of Fast Fourier Transform for the estimation of power spectra: A method based on time averaging over short, modified periodograms," *IEEE Trans. audio Electroacoust.*, vol. AU-15, no. 2, pp. 70–73, 1967.

[16] W. Q. Yang and M. S. Beck, "An intelligent cross correlator for pipeline flow velocity measurement," *Flow Meas. Instrum.*, vol. 8, no. 2, pp. 77–84, 1998.

[17] M. W. Munir and B. A. Khalil, "Cross Correlation Velocity Measurement of Multiphase Flow," *Int. J. Sci. Res.*, vol. 4, no. 2, pp. 802–807, 2015.

[18] B. J. Azzopardi, L. A. Abdulkareem, D. Zhao, S. Thiele, M. J. Silva, M. Beyer, and A. Hunt, "Comparison between Electrical Capacitance Tomography and Wire Mesh Sensor Output for Air/Silicone Oil Flow in a Vertical Pipe," *Ind. Eng. Chem.*, vol. 49, pp. 8805–8811, 2010.

[19] R. W. Sillars, "The properties of a dielectric containing semiconducting particles of various shapes," *Inst. Electr. Eng. - Proc. Wirel. Sect. Inst.*, vol. 12, no. 35, pp. 139–155, 1937.

[20] M. Soleimani and W. R. B. Lionheart, "Nonlinear image reconstruction for electrical capacitance tomography using experimental data," *Meas. Sci. Technol.*, vol. 16, pp. 1987–1996, 2005.

[21] F. Dong, Y. B. Xu, L. J. Xu, L. Hua, and X. T. Qiao, "Application of dual-plane ERT system and cross-correlation technique to measure gas – liquid flows in vertical upward pipe," *Flow Meas. Instrum.*, vol. 16, pp. 191–197, 2005.

This is the accepted version of an article published in IEEE Transactions on Instrumentation and Measurement
http://dx.doi.org/10.1109/TIM.2020.3034615

[22] G. A. Johansen and P. Jackson, *Radioisotope Gauges for Industral Process Measurements*. West Sussex: John Wiley & Sons, Ltd, 2004.
[23] G. A. Johansen and E. Abro, "A new CdZnTe detector system for low-energy gamma-ray measurement," *Sensors and Actuators*, vol. 54, no. 54, pp. 493–498, 1996.
[24] R. Maad, "Design optimization of high speed gamma-ray tomography," University of Bergen, 2009.
[25] R. Maad, B. T. Hjertaker, G. A. Johansen, and Ø. Olsen, "Dynamic characterization of a high speed gamma-ray tomograph," *Flow Meas. Instrum.*, vol. 21, no. 4, pp. 538–545, 2010.
[26] B. T. Hjertaker, R. Maad, and G. A. Johansen, "Dual-mode capacitance and gamma-ray tomography using the Landweber reconstruction algorithm," *Meas. Sci. Technol.*, vol. 22, 2011.
[27] S. Kawata and O. Nalcioglu, "Constrained Iterative Reconstruction by the Conjugate Gradient Method," *IEEE Trans. Med. Imaging*, vol. MI, no. 2, pp. 65–71, 1985.
[28] GUM, "Evaluation of measurement data — Guide to the expression of uncertainty in measurement," 2008.

Stian Husevik Stavland holds an MSc from University of Bergen in Physics (2005) as well as an B.Eng in Automation from Bergen University College (2003). He has been engaged in Research & Development of measurement instrumentation for more than decade, first at Christian Michelsen Institute in Bergen Norway (CMR), later as part of the Norce research institute, before starting his PhD work at the University of Bergen (UiB). His doctoral work, in Measurement Science addresses the use of Industrial Tomography methods for multiphase processes measurements.

Yessica Arellano received her BE and M.Sc. degrees from La Universidad del Zulia in 2005 and 2011 respectively. A second M.Sc. with distinction was awarded by the Robert Gordon University, UK in 2008. Her doctoral research in Fluid and Complex Systems from Coventry University, UK (2020), targeted tomography measurements of multiphase flow. For 11 years, she worked within the Oil and Gas Industry, initially in offshore facilities and later as a R&D Engineer in fluid mechanics at INTEVEP S.A. Currently, she is a Research Scientist in SINTEF Energi AS.

Andy Hunt received his BSc degree in Aeronautical Engineering from the University of Bristol (UK) in 1978, and his PhD in aerodynamics from Cranfield University (UK) in 1982. He is Professor of Oil and Gas Engineering at Coventry University, Technical Director at iPhase Ltd, and CEO of Atout Process Ltd, all in the UK. After being post-doctoral research fellow and lecturer at the University of Surrey he spent 15 years in the oil industry with Schlumberger, one of the world's 'big three' oilfield service companies where he was Head of Fluid Dynamics Research and Product Development Director. Andrew Hunt is a Chartered Engineer, Fellow of the Institute of Measurement and Control, and has been visiting professor at the University of Manchester (1996 to 2002) and vice-President of the Institute of Measurement and Control (2002-2007).

Rachid Maad received his Ph.D. in physics from the University of Bergen, Norway in 2009, Thesis: **"***Design optimization of high speed gamma-ray tomography***",** Department of Physics and Technology, University of Bergen, Norway. He is working as senior engineer at the University of Bergen.

Bjørn Tore Hjertaker received the Dr. Sci. degree (Ph.D.) from the University of Bergen, Bergen, Norway, in 1998, for research on dual mode tomography. He is a Professor with the Department of Physics and Technology, University of Bergen. His main fields of interest are electromagnetic and nucleonic instrumentation and their industrial applications, particularly in multiphase hydrocarbon flow and separator level measurement. Previously, he was a Scientist with ABB Corporate Research Norway (Department of Oil and Gas), and Christian Michelsen Research AS (Department of Industrial Instrumentation). He has also been with Haukeland University Hospital, Bergen, as a Medical Physicist within hyperthermia cancer treatment.

This is the accepted version of an article published in IEEE Transactions on Instrumentation and Measurement
http://dx.doi.org/10.1109/TIM.2020.3034615